technologies

MDPI

Article

Enhancing Areal Density Based on Signal Processing Techniques in Staggered Dual-Layer Bit-Patterned Magnetic Recording Systems

Natthakan Rueangnetr [1], Satra Tor. Wattanaphol [1], Santi Koonkarnkhai [2], Simon John Greaves [3] and Chanon Warisarn [1,*]

[1] School of Integrated Innovative Technology, King Mongkut's Institute of Technology Ladkrabang, Bangkok 10520, Thailand; natthakan.ru@kmitl.ac.th (N.R.); 68236013@kmitl.ac.th (S.T.W.)
[2] Faculty of Science and Technology, Nakhon Pathom Rajabhat University, Nakhon Pathom 73000, Thailand; santi@npru.ac.th
[3] Research Institute of Electrical Communication (RIEC), Tohoku University, Sendai 980-8577, Japan; simon@riec.tohoku.ac.jp
* Correspondence: chanon.wa@kmitl.ac.th; Tel.: +66-86-997-1001

Abstract

Dual-layer bit-patterned magnetic recording (DL-BPMR) is a promising approach to extend areal-density scaling by exploiting the vertical dimension; however, reliable retrieval is challenged by the inherently weaker lower-layer readback and additional interference mechanisms, inter-symbol interference, inter-track interference, and inter-layer interference, that distort the mixed readback signal. This study presents a co-designed dual-layer BPMR scheme with an areal density of 2.0 to 6.0 Terabits per square inch (Tbits/in^2), based on two complementary approaches. First, we vary the head–media spacing (HMS) to reduce the distance between the read head and the recording layers, especially the lower layer, strengthening the lower-layer contribution and making the mixed readback clearer and more reliable. Second, conditioned-HMS readback is processed using a combined-processing receiver tailored to a staggered (down-track-offset) dual-layer layout, where oversampling enables a unified one-dimensional sequence representation for dual-layer detection without enforcing early layer separation. To further improve detection efficiency, we also introduce a two-step minimum mean square error design that first determines a short monic generalized partial response target and then computes a minimum mean square error equalizer matched to the resulting readback, producing an equalized sequence suitable for soft-output sequence detection and low-density parity-check coded decoding. The simulation results indicated that reducing the head-media spacing improves readback separability (i.e., reliability) and that the proposed two-step combined-processing partial-response maximum-likelihood method achieves a consistently lower mean-squared error than conventional dual-layer processing across signal-to-noise ratios (SNRs). More importantly, in end-to-end bit-error-rate (BER) evaluation under electronic noise, e.g., the proposed dual-layer BPMR system delivers a clear reliability advantage over a single-layer BPMR baseline, achieving SNR gains of 4.2 dB at BER = 10^{-4} and 3.7 dB at BER = 10^{-5} in the favorable head-media spacing regime, thereby demonstrating robust high-density dual-layer retrieval beyond the single-layer baseline.

Keywords: dual-layer bit-patterned magnetic recording; head–media spacing; combined processing; generalized partial response; minimum mean square error equalization; inter-layer interference

Check for updates

Academic Editor: Hongying Meng

Received: 29 September 2026
Revised: 27 October 2026
Accepted: 3 November 2026
Published: 5 November 2026

Copyright: © 2026 by the authors. Licensee MDPI, Basel, Switzerland. This article is an open access article distributed under the terms and conditions of the Creative Commons Attribution (CC BY) license.

1. Introduction

Driven by the exponential growth in demand for large-capacity data storage, hard disk drives (HDDs) remain a primary technology in data centers and storage infrastructure. Perpendicular magnetic recording (PMR) has been the dominant standard for the past two decades, achieving areal densities (AD) of up to approximately Terabits per square inch (Tbits/in^2). However, to overcome the superparamagnetic limit of conventional PMR and support data-intensive applications, HDD technology must transition toward significantly higher AD capabilities. Heat-assisted magnetic recording (HAMR) [1–3] and microwave-assisted magnetic recording (MAMR) [4–6] have emerged as two key energy-assisted technologies to meet these demands. Nevertheless, both approaches present critical practical challenges when writing to high-anisotropy granular media. HAMR requires precise thermal management to prevent laser-induced heat from degrading drive reliability, while MAMR faces substantial design and power constraints in implementing a functional spin-torque oscillator within the compact write head.

An alternative and highly promising recording technology is bit-patterned magnetic recording (BPMR) [7–10], which replaces granular media with a well-ordered array of lithographically patterned, isolated magnetic islands. Because each island can be larger than a single grain in conventional media, BPMR can provide improved thermal stability while maintaining compatibility with writer structures similar to those used in current HDDs. Beyond the conceptual advantages of patterned islands, continued progress in bit-patterned media (BPM) fabrication has strengthened BPMR feasibility. For example, ref. [11] proposes a method for fabricating BPM using a CoCrPt alloy. This approach combines multiple techniques, including rotary-stage electron-beam lithography, directed self-assembly of block copolymers, self-aligned double patterning, nanoimprint lithography, and ion milling, and has demonstrated ADs up to 1.6 Tbits/in^2. Importantly, BPMR is a crucial technology not only for single-layer systems but also for future multi-layer architectures, where interlaced or staggered bit-patterned layouts can be implemented to exploit both lateral and vertical dimensions for data storage, as reflected in recent roadmap and comparative media analyses [12].

To further surpass the superparamagnetic limit while continuing AD scaling, multi-layer extensions of BPMR have been considered. A combination of BPMR and multi-layer magnetic recording (MLMR) concepts, often referred to as multi-layer BPMR (ML-BPMR) [13,14], has been introduced as a pathway toward extremely high AD by stacking multiple recording layers, thereby leveraging both horizontal and vertical dimensions. In this paper, we focus specifically on the dual-layer case, i.e., dual-layer BPMR (DL-BPMR), which represents a practically relevant step toward general ML-BPMR and already encapsulates the key challenges of multi-layer readback. While DL-BPMR can significantly enhance AD, reliable data retrieval becomes substantially more difficult because the readback waveform is a superposition of contributions from two physically separated layers. One of the main issues is the inherent difficulty of retrieving data from the lower recording layer due to its increased distance from the read/write head, as conceptually illustrated in Figure 1. In addition, wide reader sensitivity can lead to severe inter-symbol interference (ISI) and inter-track interference (ITI), degrading signal integrity. Furthermore, inter-layer interference (ILI), arising from magnetic interactions and coupled readback contributions during the reading process, further complicates detection by distorting the observed waveform. Consequently, effective media-structure and receiver designs (signal-processing methods) that can robustly recover data from both the upper and lower layers, under practical interference and noise conditions, are essential to enabling DL-BPMR systems at high AD.

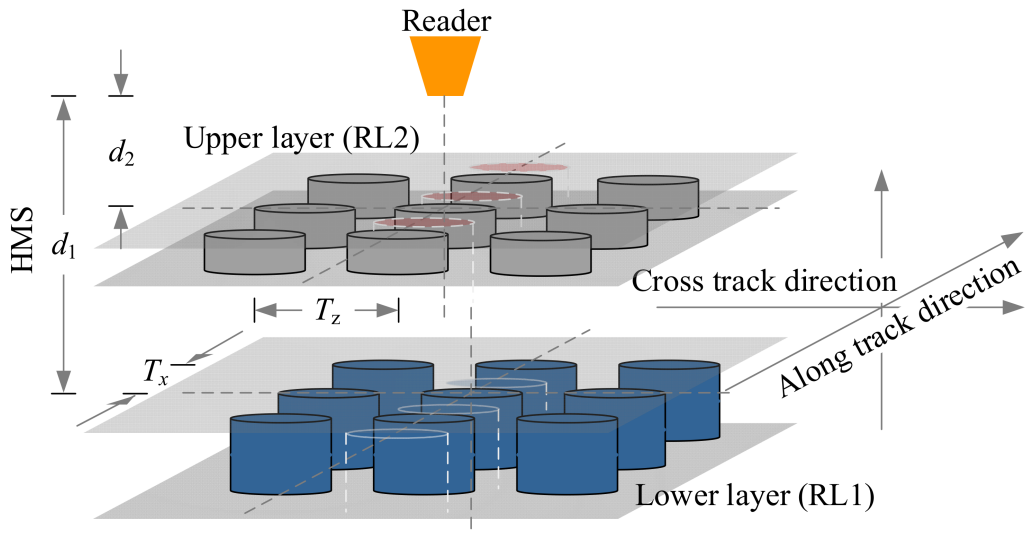


Figure 1. Cartoon representation of the dual-layer BPMR structure and reader sensitivity for the upper and lower recording layers.

Several studies have addressed DL-BPMR challenges through two complementary directions: media-structure design and receiver design. On the media side, dual-layer BPMR configurations in which the centers of lower-layer islands are positioned in the gaps of the upper layer are presented in [15], deliberately introducing layer misalignment to create more structured dual-layer readback contributions and enabling receiver designs that explicitly incorporate both layers. In addition, ref. [16] optimized the thicknesses of the dual recording layers and demonstrated that layer thickness can strengthen the weaker lower-layer contribution and improve the balance between upper- and lower-layer readback responses, which is critical for reliable DL operation. Beyond layout and thickness, prior studies have identified head–media spacing (HMS) as a primary factor in multi-layer recording, since increasing HMS reduces the lower-layer readback amplitude and makes the mixed readback more ambiguous. Prior DL and multi-layer studies have consistently shown that the head-to-layer separation is a major readback bottleneck. For example, ref. [17] emphasized that the head-to-layer distance directly limits lower-layer visibility in DL readback and can dominate retrieval difficulty when the mixed signal is strongly coupled. Building on this observation, ref. [18] examined layer-thickness and geometry tuning under controlled spacing and showed that media-structure optimization can rebalance upper- and lower-layer readback strengths, improving lower-layer contribution without destabilizing the composite response.

Related investigations in [19] further demonstrated that geometric design choices in DL media (e.g., staggered/overlapping layouts or other structured arrangements) can reshape the mixed readback into a more tractable form for downstream detection by reducing severe simultaneous overlap between layer contributions. From a practical head/spacing sensitivity standpoint, ref. [20] experimentally confirmed that reducing HMS improves readability (and writability) under tight signal-margin conditions, directly validating HMS as a key lever for strengthening readback. These findings are consistent with roadmap guidance in [21], which highlights increasingly stringent HMS control as a requirement for continued HDD scaling toward aggressive density targets. Collectively, these results motivate treating HMS as an explicit design variable in DL-BPMR evaluation and receiver design, rather than a fixed nuisance parameter, particularly when robust detection must operate on a strongly coupled dual-layer readback mixture.

On the receiver side, ref. [22] proposed a multi-dimensional signal-processing framework for dual-layered bit-patterned media, where coupled readback sequences

are detected in a structured manner (e.g., sequential/multi-track detection) to mitigate multi-dimensional interference and improve retrieval reliability in high-density operation. Ref. [23] investigated iterative signal-processing schemes for dual-layered BPMR in which partial response maximum likelihood (PRML)-based processing is applied to recover layer information in an iterative fashion, using intermediate decisions to reproduce layer-wise contributions and refine detection with targets/equalizers matched to each reproduced readback component, thereby improving bit-error-rate (BER) relative to a single-layer baseline at the same total user density (UD). Advanced DL-BPMR detection was achieved by introducing a maximum a posteriori (MAP)-based detector built on a validated DL-BPMR channel model [24], demonstrating that MAP/extrinsic information processing can improve BER over conventional Viterbi-based detection by more effectively exploiting the coupled nature of the dual-layer readback during soft-information generation. Ref. [25] focused explicitly on ILI and proposed an ILI-suppression approach combined with sum-soft-information (SSI) processing that strengthens bottom-layer reliability via log-likelihood ratio (LLR) aggregation and then feeds back the refined information to reduce interference in the top-layer readback, demonstrating significant BER gains over both single-layer-BPMR (SL-BPMR) and standard DL-BPMR in high-density conditions.

Motivated by these observations, and by increasing evidence that DL-BPMR performs best when the media structure and the receiver are jointly designed, this study presents a unified DL-BPMR framework built on two approaches that work as a single system. First, we vary the HMS under the proposed dual-layer media structure to strengthen the lower-layer (RL1) readback by reducing the head-to-layer distance. To study the spacing effect in a controlled way, HMS is swept while the inter-layer spacing is adjusted to maintain a constant overall head-to-soft underlayer (SUL) distance. This controlled spacing strategy improves the balance between upper- and lower-layer contributions, producing a clearer, more reliable mixed readback signal. Second, we turn this HMS-conditioned readback into reliable bit decisions using a combined signal-processing framework designed specifically for a staggered (down-track-offset) dual-layer island layout. The staggered geometry, together with oversampling, allows the mixed readback to be mapped into a single one-dimensional interleaved sequence, so PRML-based sequence detection can operate directly on the coupled dual-layer response without forcing early layer-by-layer separation. Within this combined-processing framework, we apply a two-step MMSE target/equalizer design to obtain a pair of target and equalizer that better match the resulting readback condition, thereby improving receiver robustness compared with conventional one-shot designs. The proposed framework is evaluated at an areal density (AD) of 4.0 Tbits/in^2 under practical interference and noise using a low-density parity-check (LDPC)-assisted iterative detection-and-decoding setup, with controlled decoding settings to highlight the effectiveness of the proposed combined-processing PRML receiver.

The key advantage of the proposed system lies in the joint design of the dual-layer media structure and the signal-processing receiver. Reducing the HMS strengthens and sharpens the readback responses, particularly the weaker lower-layer contribution. At the same time, the staggered half-bit-offset arrangement produces a more structured overlap between the upper- and lower-layer signals. With an appropriate HMS, the amplitudes of the two-layer contributions become more balanced, resulting in a clearer and more reliable mixed readback waveform. Because this waveform directly reflects both the recorded data and the effective physical channel, it is used to derive the GPR target in the first step of MMSE design. The resulting channel-aware target provides a realistic desired response for sequence detection and is subsequently used to design the FIR equalizer in the second step of MMSE design. This media–receiver co-design reduces target–equalizer mismatch and

enables the receiver to exploit the improved readback condition, leading to lower MSE and BER than conventional dual-layer processing.

Below, we summarize the main contributions of this paper:

- HMS-based readback strengthening for clearer DL signals: We sweep the HMS to bring the reader closer to the recording layers, especially the lower layer, while adjusting the interlayer spacing to keep the overall head-to-SUL distance constant. This controlled adjustment isolates the HMS effect, strengthens the lower-layer contribution, and improves the balance between upper- and lower-layer responses, yielding a clearer, more reliable mixed readback signal for DL detection.
- Combined-processing formulation matched to staggered DL media: We exploit a staggered (down-track offset) dual-layer island layout, together with oversampling, to construct a unified one-dimensional interleaved sequence representation, which enables DL readback to be processed within a single PRML framework without imposing early-layer separation.
- Two-step MMSE target/equalizer design for better receiver matching: Within the combined-processing PRML receiver, we introduce a two-step MMSE design that (i) selects a short monic generalized partial response (GPR) target and then (ii) designs an MMSE equalizer that best realizes the target-shaped desired sequence, which produces a better-matched target–equalizer pair than conventional one-shot designs.
- Improved soft information and stronger LDPC-assisted performance: The improved target/equalizer matching yields more reliable soft outputs for the decoder, thereby enhancing LDPC-assisted iterative detection-and-decoding performance under practical interference and noise conditions.

This paper is organized as follows: Section 2 introduces the dual-layer BPMR model. Section 3 details the design of the proposed systems. Section 4 presents the numerical results, while Section 5 offers the paper's conclusion.

2. Recording Channel Model

The proposed DL-BPMR medium, illustrated in Figure 2, consists of an upper patterned recording layer (RL2) and a lower patterned recording layer (RL1) separated by a non-magnetic interlayer. Table 1 summarizes the geometric and system parameters used to generate the patterned medium. The soft underlayer (SUL) thickness is 300 nm, the lower-layer thickness is 8 nm (RL1), the upper-layer thickness is 3 nm (RL2), and the interlayer-2 thickness is 1 nm (IL2). The patterned islands have a diameter D = 10 nm, a bit period $T_x = 18$ nm, and a track pitch $T_z = 18$ nm, corresponding to an AD of 4.0 Tbits/in^2. Additionally, the UD reported in this study refers to the total UD of each recording system. In the SL system, the entire UD is assigned to a single recording layer. In contrast, in the DL system, the same total UD is distributed equally between the upper and lower recording layers, UD = $\mathrm{UD_{up}}$ + $\mathrm{UD_{lw}}$, where $\mathrm{UD_{up}}$ and $\mathrm{UD_{lw}}$ represent the UD of the upper and lower layers, respectively. For instance, a total UD of 4.0 Tbits/in^2 corresponds to 4.0 Tbits/in^2 in the SL system, whereas it is 2.0 Tbits/in^2 per recording layer in the DL system.

A key design variable in this work is the HMS, defined as the distance between the read head's air-bearing surface (ABS) and the medium surface, as depicted in Figure 2. We sweep HMS ($p = 5, 4, 3$ nm) and adjust IL1 accordingly to keep the reader-to-SUL distance constant, thereby strengthening RL1 readback and producing a clearer, better-balanced mixed waveform for the combined-processing receiver. The read head is modeled using a reader sensitivity function with a size of 60 × 60 nm, and the simulated medium contains $N = 2040$ bits per track across 5 tracks. The DL-BPMR channel is illustrated in Figure 3. Two independent user bit sequences, denoted by u_k^{up} and $u_k^{\mathrm{lw}} \in \{1, 0\}$, representing the k-th user bit, are generated for the upper and lower recording layers, respectively. Each sequence

is encoded by an LDPC encoder [26,27] to produce bipolar coded sequences, $a_{k'}^{up}$ and $a_{k'}^{lw}$ of the k'-th coded bit, belonging to the set $\{\pm 1\}$, which are recorded onto two separated recording layers, where $a_{k'}^{up}$ was recorded into the upper layer (recording layer 2: RL2) while $a_{k'}^{lw}$ was recorded into the lower layer (recording layer 1: RL1), respectively.

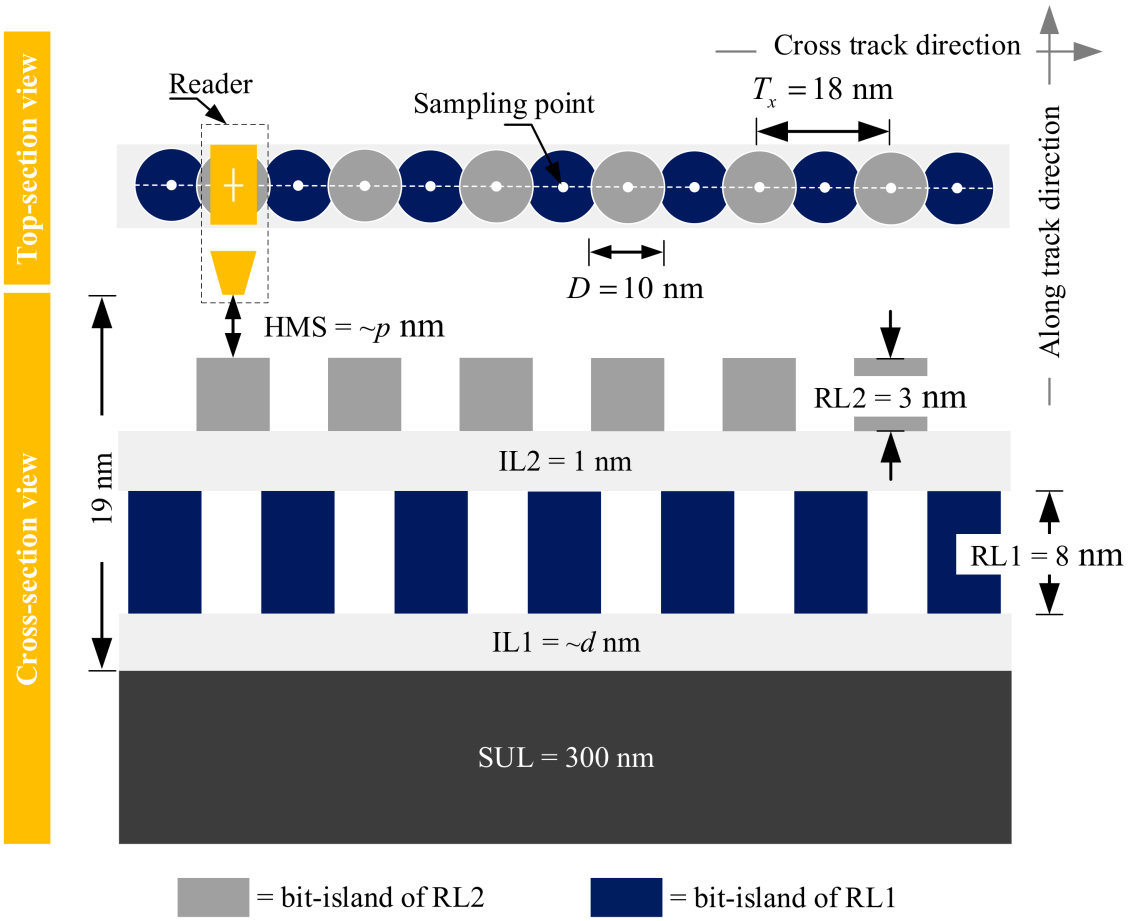


Figure 2. Schematic diagram of the DL-BPMR media consisting of cross-section and top-section views.

Table 1. Parameters used to generate bit-patterned media for dual-layer recording.

Parameters	Value
Areal density (AD)	4.0 Tbits/in^2
Bit length (T_x)	18 nm
Track pitch (T_z)	18 nm
Bit diameter (D)	10 nm
Media thickness (RL)	
Upper layer: RL2	3 nm
Lower layer: RL1	8 nm
Interlayer thickness (IL)	
Interlayer 1: IL1	~d nm (d = 2, 3, and 4 nm)
Interlayer 2: IL2	1 nm
Head media spacing (HMS)	~p nm (p = 5, 4, and 3 nm)
Soft under-layer thickness (SUL)	300 nm
Number of bits per track (N)	2040
Number of tracks	5
Reader sensitivity function size	60 nm × 60 nm

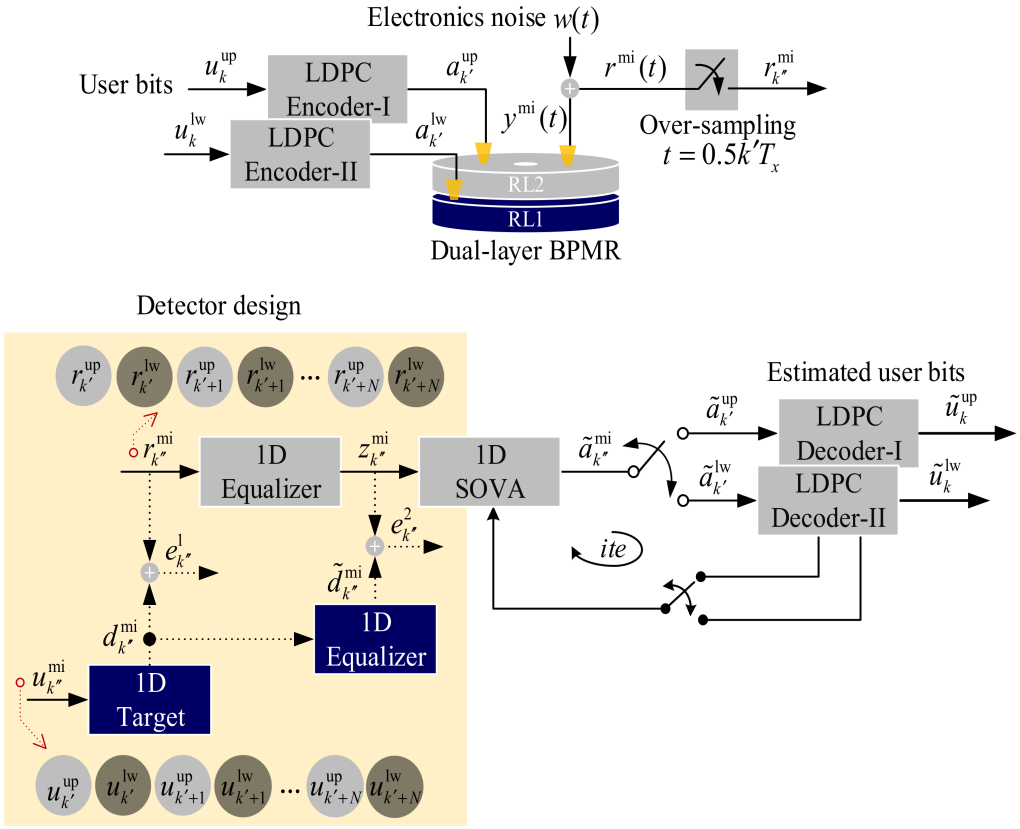


Figure 3. Block diagram of the DL-BPMR channel model, displaying the transmitter and the receiver, which represents the two-step target/equalizer design for the interleaved DL response.

It is important to note that the proposed system utilizes a regular (3,27) LDPC code with a code rate (R) of 0.889. The LDPC encoder is implemented using a parity-check matrix with 3 ones per column and 27 ones per row. This matrix is constructed based on the modified array code (MAC) [27]. It is assumed that the input sequences are randomly generated with equal probabilities of "+1" and "−1." This regular (3,27) LDPC code is used as a representative high-rate coding configuration. Its variable-node and check-node degrees are 3 and 27, respectively, giving a design code rate of $R = 8/9 \approx 0.889$. The same code and decoding settings are used for all receiver configurations so that the performance comparison focuses on the effects of the readback channel and receiver design. Here, the superscripts 'up' and 'lw' indicate the upper and lower layers, respectively. In this work, we assume flawless writing, thereby disregarding any effects that may arise from imperfect writing. The proposed DL-BPMR medium adopts a staggered island arrangement, where the island centers of the two layers are intentionally down-track offset (approximately half a bit period) rather than perfectly aligned, as illustrated in Figure 2. This staggered geometry regularizes the temporal overlap between the layer contributions: instead of producing a strongly simultaneous superposition, it induces a structured alternation in the readback dominance across sampling positions. As a result, the staggered layout naturally supports the combined processing formulation used in this study, enabling a unified one-dimensional sequence representation (e.g., via interleaving) that is more amenable to PRML-based detection and subsequent decoding.

During data retrieval, a single read head is positioned above the track center aligned to RL2, as shown in Figure 2. The read head's sensitivity is assumed to be known and modeled by a two-dimensional (2-D) response function; the spacing to each layer is implicitly captured through the corresponding layer-dependent sensitivity response. The readback signal from the j-th layer can be modeled as a 2-D convolution of the layer magnetization pattern

with the read-head sensitivity function [28]. Let x and y denote the down- and cross-track coordinates of the read head center, respectively. The continuous readback signal from the layer $j \in \{\text{up}, \text{lw}\}$ is written as

$$r^j(x,y) = \iint_S m^j(\xi,\eta)\tilde{h}^j(x-\xi, y-\eta)d\xi d\eta, \tag{1}$$

where S is the integration region centered at (x,y), $m^j(\xi,\eta) \in \{+1,-1\}$ represents the magnetization of the j-th layer over the down- and cross-track coordinates (ξ,η), and $\tilde{h}^j(x-\xi, y-\eta)$ is the layer-dependent read head sensitivity response. In the DL-BPMR system, $\tilde{h}^{\text{up}}(x-\xi, y-\eta)$ and $\tilde{h}^{\text{lw}}(x-\xi, y-\eta)$ generally differ because the effective spacing between the two layers varies; therefore, varying HMS not only alters the overall amplitude but also affects the effective pulse shape of each layer. The noise-free mixed readback signal in the time domain, here represented with parameter t, is first obtained by combining the readback responses from the upper and lower recording layers as

$$r_0^{\text{mi}}(t) = r^{\text{up}}(t) + r^{\text{lw}}(t), \tag{2}$$

where $r^{\text{up}}(t)$ and $r^{\text{lw}}(t)$ represent readback signals obtained from the upper and lower recording layers, respectively. For the BER-versus-SNR evaluation, the noise-free mixed readback signal is normalized to unit peak amplitude as

$$\bar{r}_0^{\text{mi}}(t) = \frac{r_0^{\text{mi}}(t)}{\max\left(\left|r_0^{\text{mi}}(t)\right|\right)}, \tag{3}$$

where $\max(\cdot)$ is an operator denoting the maximum element and $|\cdot|$ is the absolute value operator. The noisy mixed readback signal can then be expressed as

$$r^{\text{mi}}(t) = \bar{r}_0^{\text{mi}}(t) + w(t), \tag{4}$$

where $w(t)$ is zero-mean AWGN with variance σ^2. In this work, the signal-to-noise ratio (SNR) is expressed by

$$\text{SNR} = 10\log_{10}\left(A/\sigma^2\right), \tag{5}$$

in decibels (dB), where $A = 1$ is the normalized peak amplitude of the readback signal. Because each noise-free mixed readback waveform is normalized before AWGN is added, the BER-versus-SNR comparison primarily reflects differences in waveform shape, upper–lower recording layer balance, interference characteristics, symbol separability, and receiver matching. The absolute readback-amplitude variation caused by HMS is evaluated separately using the unnormalized readback-amplitude distributions.

The noisy readback signal was oversampled at a rate of $0.5k'T_x$ according to the bit-island arrangement, as shown in Figure 2. To exploit the staggered layout, the mixed readback signal is oversampled at half the bit period. Let T_x denote the bit period or bit length in the down-track direction. The discrete-time mixed readback sequence is obtained by oversampling the mixed readback signal as follows:

$$r_{k''}^{\text{mi}} = r^{\text{mi}}(t)\big|_{t=0.5k'T_x}, \tag{6}$$

where k'' represents the k''-th bit of the discrete-time mixed readback sequence, which is two times longer than the coded sequence in each layer. With the staggered island placement as shown in Figure 2, oversampling at $0.5k'T_x$ yields alternating sampling positions that align more strongly with one layer's island centers at a time, which motivates a combined processing representation in which the coded bits from the two layers are arranged into a single interleaved sequence. Specifically, we define an interleaved coded sequence $a_{k''}^{\text{mi}}$ such that the upper- and lower-layer coded symbols occupy alternating indices,

$$a_{2k'}^{\text{mi}} = a_{k'}^{\text{up}} \text{ and } a_{2k'+1}^{\text{mi}} = a_{k'}^{\text{lw}}. \tag{7}$$

Using the same sampling structure, the oversampled mixed readback in (4) is represented by a discrete-time sequence $r_{k''}^{\mathrm{mi}}$, which corresponds to the superposition of the two-layer readback contributions plus AWGN. Under this interleaving, the DL-BPMR retrieval task can be treated as a unified one-dimensional sequence detection problem operating directly on the coupled dual-layer response, rather than enforcing early layer-by-layer separation. The mixed oversampled discrete-time readback sequence, $r_{k''}^{\mathrm{mi}}$, was processed by the proposed one-dimensional partial response maximum likelihood (1-D PRML) to produce an equalized sequence, $z_{k''}^{\mathrm{mi}}$, which was then sent to a maximum-likelihood sequence detector; here, we employed a soft-output Viterbi algorithm (SOVA) [29] to generate reliability information in the form of log-likelihood ratios (LLRs) for the interleaved coded bits, together with the corresponding estimated interleaved coded sequence, $\tilde{a}_{k''}^{\mathrm{mi}}$. The soft-output sequence was subsequently deinterleaved into two sequences, $\tilde{a}_{k'}^{\mathrm{up}}$ and $\tilde{a}_{k'}^{\mathrm{lw}}$, which correspond to the upper and lower layers, respectively. Each sequence was decoded using an LDPC decoder [26,27] to enhance reliability and to produce the estimated user-bit sequences, $\tilde{u}_{k'}^{\mathrm{up}}$ and $\tilde{u}_{k'}^{\mathrm{lw}}$. Finally, BER is evaluated by comparing the decoded user bits with the transmitted user bits for each layer, and the overall performance is reported across the HMS settings and the media/noise conditions considered.

3. Proposed Methods

This paper proposes two complementary techniques to improve data-retrieval reliability in DL-BPMR systems: (i) readback strengthening through HMS variation and (ii) a combined-processing PRML receiver with a two-step MMSE target/equalizer design tailored to the proposed staggered dual-layer geometry. Together, these techniques co-design the media-induced effective channel and the receiver structure, making the mixed dual-layer readback more distinguishable and, therefore, more robust for sequence detection and LDPC-assisted decoding. Here, the proposed media structure and receiver are designed as complementary components. HMS reduction and staggered bit-island placement enhance the reliability of mixed readback, after which the two-step MMSE receiver derives a channel-aware target and designs an equalizer tailored to it.

To isolate the impact of HMS on DL readback while maintaining a consistent overall head-to-SUL distance, we jointly vary the HMS and the interlayer-1 thickness (IL1, denoted as d) such that the distance between the reader's lower surface and the SUL's upper surface remains fixed at 19 nm, as shown in Figure 2. Under this controlled geometry, Section 3.1 evaluates how HMS variation improves readback clarity and interference characteristics. In contrast, Section 3.2 presents the proposed combined-processing PRML receiver and its two-step target/equalizer design, explicitly matched to the resulting effective DL readback condition.

3.1. Impact of Head–Media Spacing on Readback Reliability

This study evaluates the readback characteristics of the proposed DL-BPMR media at HMS values of 5 nm, 4 nm, and 3 nm, referred to as Case I, Case II, and Case III, respectively. To maintain a consistent overall head-to-SUL distance while sweeping HMS, as described in Section 2, the interlayer spacing IL1 is adjusted accordingly: Case I ($p = 5$ nm, $d = 2$ nm), Case II ($p = 4$ nm, $d = 3$ nm), and Case III ($p = 3$ nm, $d = 4$ nm), where the objective is to identify an HMS region that yields more reliable dual-layer readback by improving symbol separability and alleviating effective interference mechanisms (ILI/ISI/ITI) that degrade detection. To directly assess front-end symbol reliability, we analyze the amplitude distributions of the readback samples obtained from Cases I–III, as illustrated in Figure 4. In addition, electronic noise is injected at SNR = 12 dB to reflect practical readback conditions and to test whether the resulting distributions remain distinguishable under noise. In

general, a strong overlap between the {+1, −1} symbol distributions indicates ambiguity and a higher likelihood of decision errors, whereas two distinct peaks indicate improved reliability. Figure 4 compares the distributions of readback-signal amplitudes for the three HMS cases and reveals a clear progression as HMS decreases. In Case I ($p = 5$ nm), the two symbol clusters are not well defined, and the distribution shows substantial spread with noticeable overlap between the {+1, −1} regions, as shown in Figure 4a. This behavior consists of increased spacing, which reduces effective readback strength and broadens the effective response, weakening the contrast between symbol polarities and increasing vulnerability to interference.

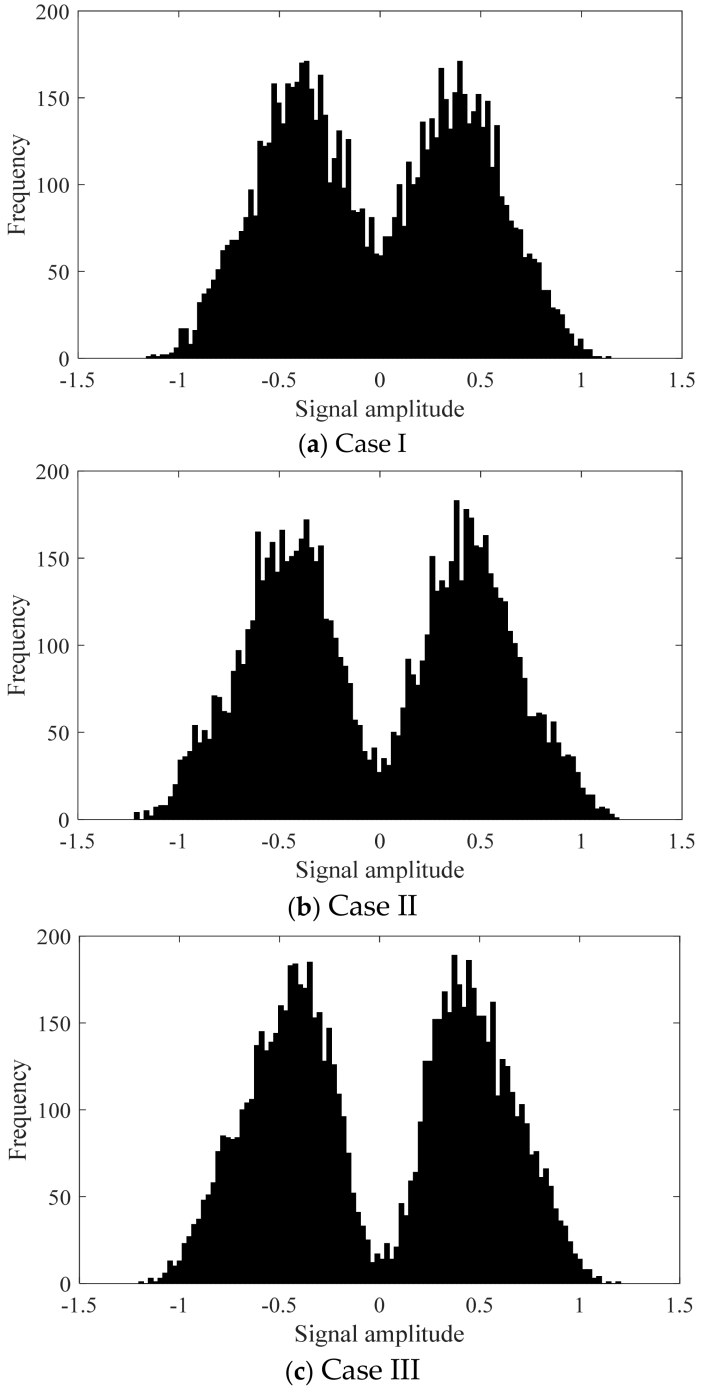


Figure 4. Signal amplitude distributions obtained from (**a**) Case-I (HMS = 5 nm), (**b**) Case-II (HMS = 4 nm), and (**c**) Case-III (HMS = 3 nm).

When HMS was reduced to 4 nm (Case II), two peak amplitudes began to emerge, and the overlap was visibly reduced, indicating that the readback amplitude became more consistent with the underlying symbol polarity, as depicted in Figure 4b. The most pronounced separation occurred for Case III (HMS = 3 nm), where two well-separated peak amplitudes were observed, providing the clearest discrimination between $\{+1, -1\}$ symbols among the tested cases, as shown in Figure 4c.

From a sequence-detection perspective, this improved separation reduces ambiguity in calculating SOVA branch metrics and typically yields more reliable soft information, particularly when the detector output is subsequently refined by LDPC decoding. While the histogram alone does not directly establish areal-density limits, it provides strong evidence that smaller HMS improves symbol reliability and readback conditioning, an essential prerequisite for robust high-AD dual-layer retrieval.

To further characterize media-induced interference, we compute waveform-based signal-to-interference ratios (SIRs) using the power definition as follows:

$$\mathrm{SIR} = 10\log_{10}(P_s/P_n), \tag{8}$$

where P_s is the power of the desired noise-free signal component, and P_n is the power associated with the interference term under consideration. Table 2 summarizes the resulting ratios for ITI and ILI across HMS values. For the single-layer (SL) baseline, the signal-to-ITI ratio increased from 9.7 dB (HMS = 5 nm) to 12.6 dB (HMS = 3 nm), indicating that smaller HMS improves the intended-track dominance relative to adjacent-track leakage. A similar improvement was observed for the DL case, e.g., from 1.1 dB to 6.8 dB as HMS decreased from 5 nm to 3 nm, consistent with stronger, more localized effective readback in the presence of dual-layer coupling. For DL inter-layer interference, the signal-to-ILI ratio also improved as HMS decreased, e.g., from 2.7 dB to 4.3 dB between 5 nm and 3 nm. Still, the absolute values confirm that residual coupling remains non-negligible.

Table 2. The SIRs are associated with the characteristics of the recording media.

Recording Media	Characteristic (dB)	
	Inter-Track Interference (ITI)	**Inter-Layer Interference (ILI)**
SL [a]		
HMS = 3 nm	12.6	-
HMS = 4 nm	11.0	-
HMS = 5 nm	9.7	-
DL [b]		
HMS = 3 nm	6.8	4.3
HMS = 4 nm	2.3	3.5
HMS = 5 nm	1.1	2.7

[a] Single-layered media. [b] Dual-layered media.

3.2. Signal Processing Technology

The results in Section 3.1 indicate that HMS variation improves the conditioning of the mixed DL readback; however, residual DL coupling and interference remain non-negligible. To reliably recover both layer sequences under such conditions, this study adopts a combined-processing receiver that explicitly matches the effective DL channel induced by the proposed staggered media geometry and the chosen HMS. Rather than separating the two layers and processing them independently, the proposed receiver treats the readback as a single structured sequence detection problem and applies a PRML-based chain with a two-step target/equalizer design to improve target–equalizer compatibility as illustrated in Figure 5.

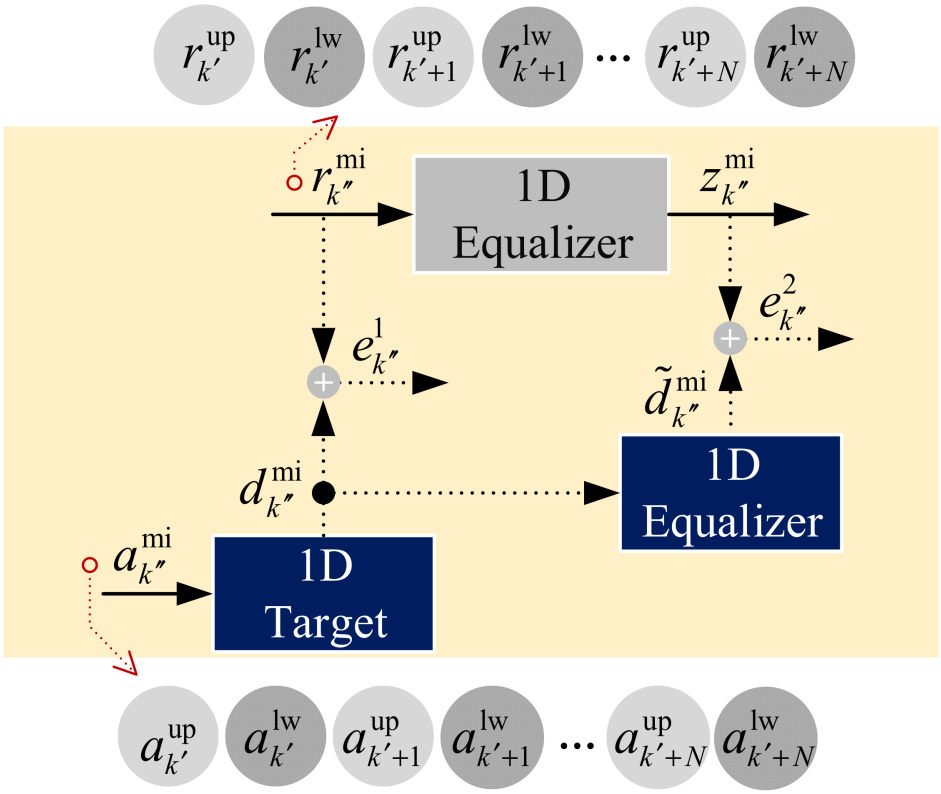


Figure 5. Block diagram of the two-step 1-D MMSE target and equalizer design for combined dual-layer processing.

Let the interleaved coded sequence, $a^{\text{mi}}_{k''}$, and the corresponding discrete-time mixed readback sequence, $r^{\text{mi}}_{k''}$, be as described in Section 2. The proposed PRML front end consists of two steps: **Step 1** (**MMSE-I**): the constrained target is designed from the mixed readback, and **Step 2** (**MMSE-II**): the equalizer is designed by using the target-shaped sequence, which can be described as follows:

As illustrated in Figure 5, we have employed a 5-tap ($L = 5$) generalized partial-response (GPR) target according to the following equation,

$$\mathbf{g} = [g_{-2}\, g_{-1}\, g_0\, g_1\, g_2]^{\mathrm{T}} \in \mathbb{R}^5, \tag{9}$$

where $[\cdot]^{\mathrm{T}}$ is the transpose operator. To avoid the trivial scaling solution and to fix the target gain, a monic constraint is imposed by setting the center tap to unity, $g_0 = 1$. In compact form, it can be defined as the column vector $\mathbf{I} = [0\ 0\ 1\ 0\ 0] \rightarrow \mathbf{I}^{\mathrm{T}}\mathbf{g} = 1 = g_0$. For each time index k'', we can define the 5-dimensional interleaved column vector of the input sequence as,

$$\mathbf{a}_{k''} = \left[a^{mi}_{k''+2}\, a^{mi}_{k''+1}\, a^{mi}_{k''}\, a^{mi}_{k''-1}\, a^{mi}_{k''-2}\right]^{\mathrm{T}} \in \mathbb{R}^5. \tag{10}$$

So that the ideal target output or target sequence is defined as the convolution of the interleaved input $a^{\text{mi}}_{k''}$ with the target response as follows,

$$d^{mi}_{k''} = \sum_{i=-2}^{2} g_i a^{mi}_{k''-i}. \tag{11}$$

Given $d^{\text{mi}}_{k''}$, we can design a length-11 finite-impulse response (FIR) equalizer response as follows,

$$\mathbf{f} = [f_{-5} \ldots f_0 \ldots f_5]^{\mathrm{T}} \in \mathbb{R}^{11}. \tag{12}$$

The corresponding 11-dimensional column vector of the readback sequence can be defined as,

$$\mathbf{r}_{k''} = \left[r^{mi}_{k''+5} \ \ldots\ r^{mi}_{k''} \ \ldots\ r^{mi}_{k''-5}\right]^{\mathrm{T}}, \tag{13}$$

and the equalizer output, or equalized sequence, can be generated from the following equation,

$$z_{k''}^{mi} = \sum_{i=-5}^{5} f_i r_{k''-i}^{mi}. \tag{14}$$

The goal of the front end is to make the equalized sequence, $z_{k''}^{\mathrm{mi}}$, closely match the target sequence, $d_{k''}^{\mathrm{mi}}$, so that the subsequent sequence detector operates on a well-shaped effective response. A central element of the proposed receiver is a two-step MMSE design that produces a better-matched target/equalizer pair for the effective interleaved DL response than conventional one-shot designs.

Step-1 (MMSE-I): Constrained target design from the mixed readback sequence.

We first determine $\mathbf{g}$ by minimizing the mean-square error (MSE) between the mixed readback sequence with an appropriate center delay and the target-filtered symbol. For a symmetric 5-tap target, we use the natural center delay as follows,

$$\Delta_t = \frac{L-1}{2} = 2. \tag{15}$$

Define the MMSE-I error as,

$$e_{k''}^{1} = r_{k''-\Delta_t}^{mi} - \mathbf{g}^{\mathrm{T}}\mathbf{a}_{k''} = r_{k''-2}^{mi} - \mathbf{g}^{\mathrm{T}}\mathbf{a}_{k''}, \tag{16}$$

and the MMSE-I target is obtained by minimizing the MSE under the monic constraint, which can be described as follows,

$$\min_{\mathbf{g}} \mathrm{E}\left[\left|e_{k''}^{1}\right|^2\right] \text{ s.t. } \mathbf{I}^{\mathrm{T}}\mathbf{g} = 1, \tag{17}$$

where $\mathrm{E}[\cdot]$ is an expectation operator. We then define an auto-correlation matrix of the interleaved input sequence and a cross-correlation matrix of the readback sequence and the interleaved input sequence as follows,

$$\mathbf{U} = \mathrm{E}\left[a_{k''}a_{k''}^{\mathrm{T}}\right] \in \mathbb{R}^{5\times 5}, \mathbf{p} = \mathrm{E}\left[a_{k''}r_{k''-2}^{mi}\right] \in \mathbb{R}^{5}. \tag{18}$$

Expanding the MSE yields a quadratic form in $\mathbf{g}$, and solving the corresponding Lagrangian yields the closed-form monic MMSE target as follows,

$$\mathbf{g}^{\mathrm{T}} = (\mathbf{p} + \lambda\mathbf{I})^{\mathrm{T}}\left(\mathbf{U}^{-1}\right)^{\mathrm{T}}, \tag{19}$$

where the Lagrange multiplier λ can be calculated from

$$\lambda = \frac{1 - \mathbf{I}^{\mathrm{T}}\mathbf{U}^{-1}\mathbf{p}}{\mathbf{I}^{\mathrm{T}}\mathbf{U}^{-1}\mathbf{I}}. \tag{20}$$

The resulting desired sequence used in the second step is then computed as,

$$d_{k''}^{mi} = \mathbf{g}^{\mathrm{T}}a_{k''}. \tag{21}$$

This first step is critical because the effective DL channel varies with HMS and media geometry; designing the target directly from the mixed readback sequence yields a target response that more closely reflects the actual channel conditions under which the detector will operate. The correlation matrices required for MMSE target and equalizer design are estimated offline using the specified channel model, the known transmitted interleaved sequence, and the corresponding simulated readback samples. The resulting coefficients are precomputed for the characterized channel and stored at the receiver. This implies that if the considered channel changes, the correlation matrices and coefficients can be updated using a known training sequence.

Step-2 (MMSE-II): Matching the equalizer design to the target-shaped sequence.

In the second step (MMSE-II), given the target $\mathbf{g}$ obtained from Step-1 and the desired sequence $d_{k''}^{\mathrm{mi}}$, we then design the FIR equalizer coefficients, $\mathbf{f}$, to minimize the MSE between the equalizer output, $z_{k''}^{\mathrm{mi}}$ and the desired sequence, $d_{k''}^{mi}$. For the 11-tap equalizer, L_f, we align with the center of the observation window by selecting a center delay that can be defined as,

$$\Delta_e = \frac{L_f - 1}{2} = 5. \tag{22}$$

We can define the MMSE-II error as follows,

$$e_{k''}^2 = d_{k''-\Delta_e}^{mi} - \mathbf{f}^{\mathrm{T}}\mathbf{r}_{k''} = d_{k''-5}^{mi} - \mathbf{f}^{\mathrm{T}}\mathbf{r}_{k''}. \tag{23}$$

The MMSE-II equalizer is then obtained from,

$$\min_{\mathbf{f}} \mathrm{E}\left[\left|e_{k''}^2\right|^2\right]. \tag{24}$$

Then, we can define

$$\mathbf{R} = \mathrm{E}\left[\mathbf{r}_{k''}\mathbf{r}_{k''}^{\mathrm{T}}\right] \in \mathbb{R}^{11\times 11},\ \mathbf{q} = \mathrm{E}\left[\mathbf{r}_{k''}d_{k''-5}^{mi}\right] \in \mathbb{R}^{11}. \tag{25}$$

Finally, the FIR equalizer can then be calculated from the following,

$$\mathbf{f}^{\mathrm{T}} = \mathbf{q}^{\mathrm{T}}\left(\mathbf{R}^{-1}\right)^{\mathrm{T}}. \tag{26}$$

By explicitly matching the equalizer to the Step-1 target, the proposed two-step procedure improves target–equalizer compatibility and yields a more stable PRML front end across HMS conditions than one-shot designs, which may be sensitive to channel variations.

Finally, the equalized sequence $z_{k''}^{mi} = \mathbf{f}^{\mathrm{T}}\mathbf{r}_{k''}$ is processed by a soft-output sequence detector. In this work, a SOVA detector is employed to generate LLRs for detecting interleaved coded bits, which are then deinterleaved into upper- and lower-layer sequences and decoded using LDPC decoders. This soft-information flow is particularly important in the DL setting because residual ILI and ISI can still cause ambiguity even after equalization; reliable LLRs allow the LDPC decoder to exploit code constraints and correct errors that would otherwise dominate the BER floor. The step-by-step derivation of the MMSE formulations, including the target and equalizer coefficients, is provided in the Appendix A.

4. Simulation Results

This section reports the end-to-end performance of the proposed DL-BPMR framework under the controlled HMS geometry setting as described earlier. The results are organized to reflect the receiver pipeline: (i) HMS-based readback conditioning, (ii) interference characterization, and (iii) receiver effectiveness measured by target/equalizer parameters, MSE, and BER performance. Across all experiments, the key comparisons are between single-layer (SL), conventional DL processing (DL–Conv.), and the proposed DL processing (DL–Prop.). At the same time, HMS ranged from 3 nm to 5 nm across all three cases. Table 3 summarizes the representative 1-D PRML coefficients used by SL, DL-Conv, and DL-Prop at each HMS, including the 1-D equalizer coefficients and the 1-D monic GPR target coefficients.

In this study, the dimensions of the 1-D GPR target and the 1-D equalizer coefficients were set to 1 × 5 and 1 × 11, respectively. Several consistent observations can be drawn; these coefficients are influenced by HMS variation.

Table 3. Equalizer and GPR target coefficients for SL-conv., DL-conv., and Prop. DL-1-D PRML systems without media noise.

Recording Media	1-D PRML Systems	
	1-D Equalizer Coefficients	**1-D GPR Target Coefficients**
Single Layer: SL—Conv.		
HMS = 3 nm	[0.00327 −0.00058 −0.00358 0.00177 −0.00228 −0.00910 0.22717 −0.00411 −0.00958 0.00263 −0.00207]	[0.01169 0.00167 1.00000 0.00158 −0.02299]
HMS = 4 nm	[0.00521 0.00217 −0.00102 −0.00106 −0.01016 −0.01404 0.26685 −0.00131 0.00423 0.00248 −0.00042]	[0.00416 0.02409 1.00000 0.02420 0.00403]
HMS = 5 nm	[0.00572 0.00461 −0.00108 −0.00089 −0.01538 −0.00193 0.28442 0.00633 −0.00603 0.00144 0.00271]	[0.01225 0.06543 1.00000 0.06342 −0.01255]
Double Layer: DL—Conv.		
HMS = 3 nm	[−0.00008 0.00919 −0.01966 −0.01772 −0.02532 −0.02798 0.32081 1.58820 0.41075 −0.01429 −0.03889]	[0.04858 0.32177 1.00000 0.32098 0.04708]
HMS = 4 nm	[−0.00486 0.01163 −0.01775 −0.00779 −0.03894 −0.07814 0.27816 1.69988 0.39324 −0.06958 −0.05401]	[0.03401 0.32464 1.00000 0.32314 0.03162]
HMS = 5 nm	[−0.00526 0.01480 −0.01869 −0.01799 −0.05385 −0.10647 0.26787 1.81733 0.40319 −0.11518 −0.08296]	[0.03867 0.34879 1.00000 0.34623 0.03499]
Dual Layer: DL—Prop.		
HMS = 3 nm	[0.00870 −0.01251 −0.03454 −0.00785 0.11184 1.72543 0.10714 −0.01235 −0.0312 −0.00798 −0.01322]	[0.05237 0.47132 1.00000 0.53367 0.17955]
HMS = 4 nm	[0.00396 −0.01998 −0.03248 −0.03107 0.06691 1.77738 0.05049 −0.03144 −0.03626 −0.00113 −0.01704]	[0.03646 0.19883 1.00000 0.14324 0.03485]
HMS = 5 nm	[0.00124 −0.01885 −0.03677 −0.06246 −0.02598 2.04855 −0.06023 −0.05231 −0.04792 0.00365 0.01895]	[0.01104 0.24283 1.00000 0.30922 0.08996]

The above structural differences among SL, DL–Conv., and DL–Prop were reflected in the MSE performance, as illustrated in Figure 6. Here, the MSE can be computed as follows,

$$\text{MSE} = \frac{1}{N'}\sum_{k=1}^{N'}(z_k - d_k)^2, \tag{27}$$

where d_k denotes the noise-free target sequence obtained by convolving the recorded sequence with the designed GPR target, z_k is the equalized sequence, and N' is the length of the considered sequence. As the SNR increased, the SL case exhibited the smallest MSE, approaching zero in the high-SNR regime, consistent with the simpler SL readback response. In contrast, DL–Conv. showed a pronounced MSE floor even at high SNR, indicating that residual interlayer coupling/interference in the mixed DL readback prevents the conventional design from producing an equalized sequence that closely matches the intended target output d_k. Importantly, for the proposed DL–Prop., the receiver reduced this gap by yielding consistently lower MSE than DL–Conv. across all SNR and HMS values studied, with the clearest improvement appearing in the medium-to-high SNR range, where target/equalizer mismatch becomes the dominant limitation. Overall, these results confirm that the proposed receiver, via its improved target/equalizer matching, enhances equalization fidelity under the coupled DL response and produces a target-shaped sequence better suited for reliable PRML sequence detection.

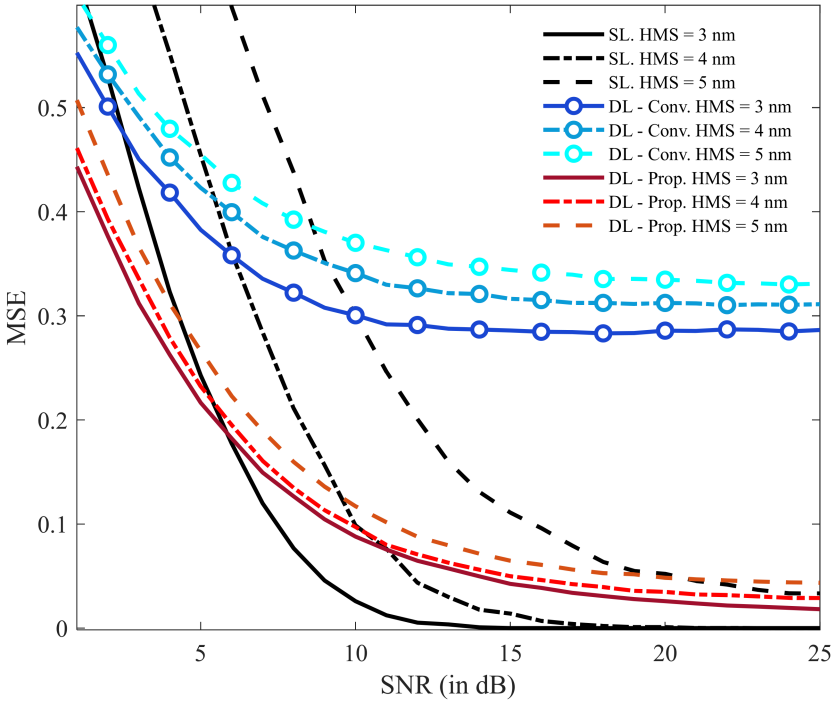


Figure 6. MSE versus SNR for the SL, conventional DL (DL–Conv.), and proposed DL (DL–Prop.) PRML systems at HMS values of 3, 4, and 5 nm.

Figure 7 provides a compact operating-point comparison by reporting the BER at a fixed SNR of 8 dB for each HMS value, thereby isolating how spacing and receiver design translate into end-to-end reliability under the same level of electronic noise. The dominant trend is spacing-driven: as HMS decreased (from 5 nm to 3 nm), the BER dropped across all schemes because smaller spacing increases the effective readback strength and sharpens the composite response, thereby improving the separability of symbol-dependent waveform patterns and reducing ambiguity in the sequence metrics used by PRML/SOVA.

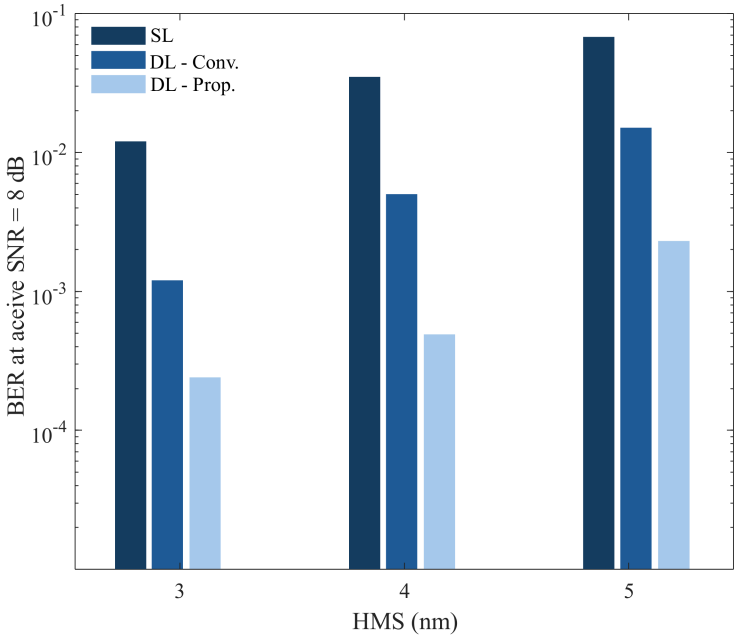


Figure 7. BER bar performances of various recording systems by fixing an SNR at 8 dB.

Under the same conditions, DL–Prop. consistently delivered the lowest BER, indicating that the proposed combined-processing PRML receiver was better matched to the coupled dual-layer signals and could convert the "HMS-conditioned" waveforms into more reliable soft information or LLRs than conventional DL processing. This advantage is most valuable when DL coupling and ILI/ISI are non-negligible, i.e., when performance is limited not only by noise but also by target/equalizer mismatch and residual interference. DL–Conv. improved over the SL baseline but remained clearly behind DL–Prop., implying that a conventional one-shot design is less effective at handling the structured superposition created by the staggered geometry. Finally, the widening BER gaps as HMS approaches 5 nm indicate that spacing-induced attenuation weakens deeper-layer readback more severely, worsening the balance between layer contributions. As a result, the mixed readback becomes more ambiguous, leaving the receiver with a smaller margin for reliably recovering the sequences at this SNR.

In Figure 8a, the BER curves without media noise reflect end-to-end reliability under electronic noise only and show three consistent behaviors across the tested conditions. First, reducing HMS improved BER for all schemes, i.e., SL, DL–Conv., and DL–Prop., confirming that smaller spacings strengthen the effective readback signal and increase the detection margin. Second, DL–Prop. consistently outperformed DL–Conv. over the SNR range, indicating that the improved equalization fidelity, as reflected by lower MSE, carried through the full PRML/SOVA/LDPC chain and produced meaningful end-to-end gains. Third, in favorable HMS regimes, the proposed DL approach provides a clear reliability advantage over the SL baseline at the same areal density, showing that once the deeper-layer visibility is strengthened by HMS conditioning and the receiver is explicitly matched to the effective coupled DL response, DL retrieval becomes not only feasible, but also can surpass SL reliability. As HMS increased, the performance gaps tended to narrow because the deeper-layer contribution became intrinsically weaker and the mixed readback signal became more ambiguous, reinforcing the main co-design message: DL gains are maximized when the physical readback condition (HMS) and the receiver design are aligned. For example, at a BER of around 10^{-4}, DL-Prop. showed improvements of 0.8 dB and 4.2 dB over DL-Conv. and SL, respectively. In this study, for each SNR point, we evaluated the BER using 49,020 independent blocks of 2040 bits, corresponding to 100,000,800 bits. The simulations terminated after reaching this predetermined number of blocks. In addition, when no errors were observed, the BER is reported as below 1.0×10^{-8}.

In Figure 8b, when media noise, such as position fluctuations, was introduced, BER degraded across all systems, reflecting the additional uncertainty caused by island-position fluctuations. However, the main ordering remained consistent, with the proposed DL–Prop remaining the best performer. The receiver maintained a clear advantage over conventional DL processing, indicating that the proposed combined-processing PRML chain is more robust to realistic distortions that appear as structured interference in the readback sequence. Moreover, the sensitivity to HMS remained evident in the presence of media noise: even with smaller spacing, BER improved, indicating that HMS-based conditioning continued to provide margin even when the readback was corrupted by both electronic noise and media-induced fluctuations. This behavior is consistent with the interpretation that HMS reduction strengthens the underlying signal structure and increases the effectiveness of subsequent sequence-based processing. However, since our proposed analysis varies HMS and the IL1 interlayer thickness simultaneously while keeping the head-to-SUL distance constant, the investigated configurations differ in more than one geometric parameter. To clarify the physical implications of this coupled variation, we have an additional study and found that reducing HMS can significantly improve BER when IL1 is fixed at 3 nm, indicating that HMS independently affects readback performance under this condition.

However, when HMS is fixed at 4 nm, the varying IL1 also affects BER. Therefore, the improvement observed in the original configurations, where HMS and IL1 were varied simultaneously, should be attributed to the combined spacing configuration rather than HMS reduction alone.

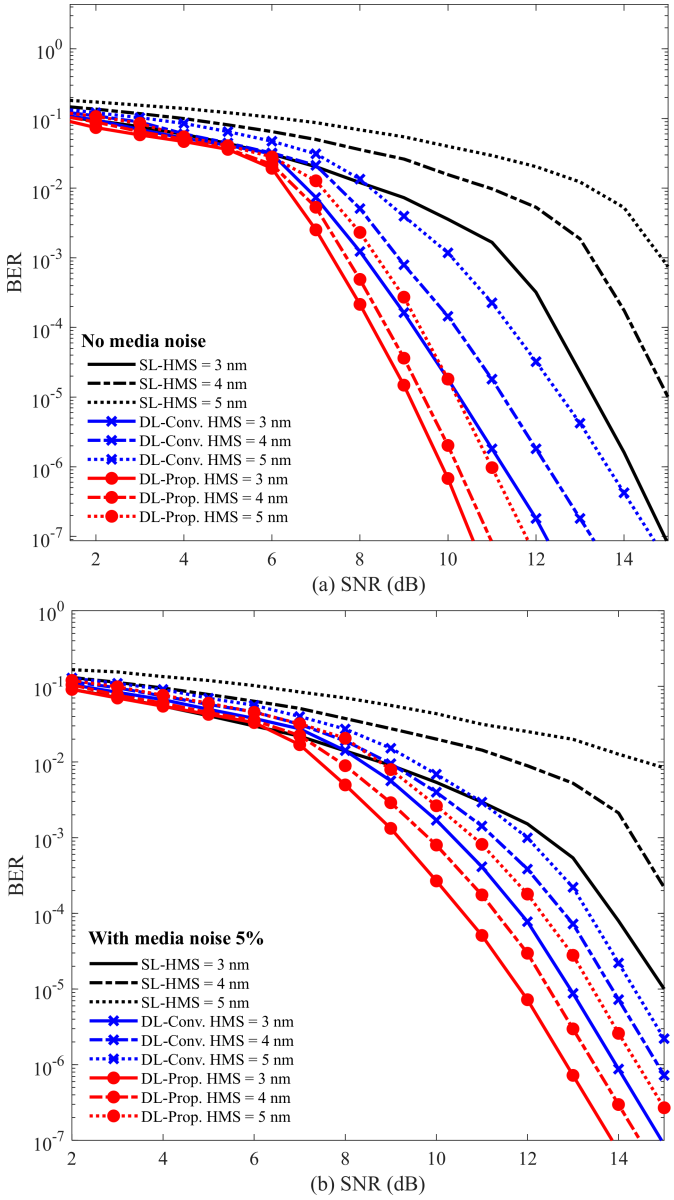


Figure 8. BER performance of the DL-Prop. technique compared with DL-Conv. and SL systems at an AD of 4.0 Tbits/in^2, (**a**) without and (**b**) with 5% media noise, respectively.

Furthermore, to provide a steadfast comparison with an interference-aware receiver, Figure 9 presents BER as a function of UD for the conventional 1-D DL-PRML, 2-D DL-PRML, and proposed receivers. The 2-D DL-PRML represents the PRML system that employed a 2-D equalizer and 2-D detector [30] to mitigate the effect of 2-D interference, i.e., ISI and ITI. The conventional 2-D PRML system can efficiently handle 2-D interference when compared with the 1-D PRML system. However, in this work, the 2-D DL-PRML is used for comparison purposes. It may not be suitable when the recording must encounter the ILI effect, as occurs in a dual-layer recording system. Here, the comparison was conducted at HMS = 3 nm, which provides the best BER performance among the HMS conditions. Using the same HMS for all receivers enables the effect of increasing UD to be evaluated independently of

HMS variation. At relatively low UDs of 2.0–3.0 Tbits/in^2, the proposed and 2-D DL-PRML receivers exhibit comparable performance, with the 2-D DL-PRML detector providing a slightly lower BER. However, from UD = 4.0 Tbits/in^2 onward, the proposed receiver achieves the lowest BER among the DL methods considered, and this advantage becomes more pronounced as UD increases. For example, at UD = 6.0 Tbits/in^2, the proposed receiver achieves a BER of approximately 6×10^{-3}, compared with approximately 1.3×10^{-2} for the 2-D DL-PRML receiver and 2.5×10^{-2} for the conventional 1-D DL-PRML receiver. These results indicate that the proposed channel-matched two-step MMSE target/equalizer design is particularly effective under high-density conditions, where ISI, ITI, and interlayer coupling become more severe. Consequently, the proposed receiver provides improved robustness for high-density dual-layer recording without requiring a multidimensional detection structure.

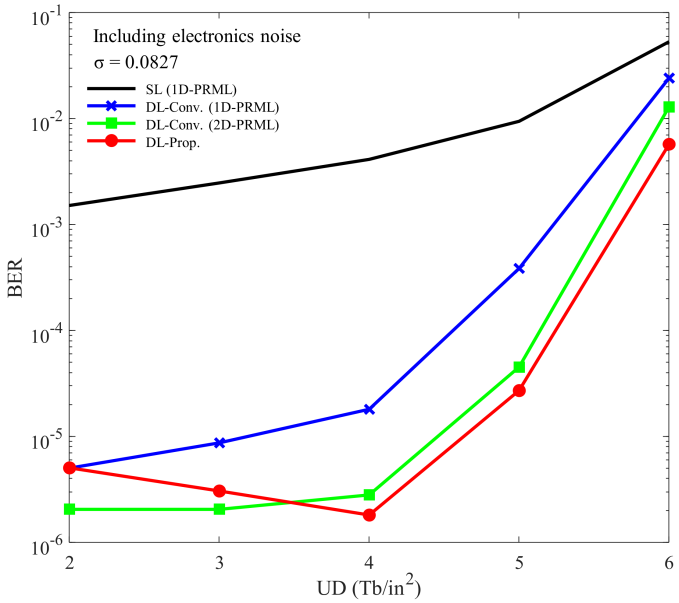


Figure 9. BER performance as a function of UD for the 1-D SL-PRML, conventional 1-D DL-PRML, conventional 2-D DL-PRML, and proposed receivers under electronic noise with $\sigma = 0.0827$ and HMS = 3 nm.

To further evaluate robustness under nonideal media conditions, Figure 10 presents BER performance for media-noise levels ranging from 2% to 10%. The BER increases with media-noise level for all considered receivers because media-induced variations distort the effective readback response and increase the uncertainty of the sequence metrics. Nevertheless, in the lower-BER operating regime, the proposed receiver maintains the lowest BER over the investigated media-noise range. At 10% media noise, the proposed receiver achieves a BER of approximately 8×10^{-3}, compared with approximately 3×10^{-2} for the referenced receivers. This result indicates that the channel-matched two-step MMSE design retains a clear reliability advantage under moderate media variations. However, under the more severe operating conditions, the BER curves converge and remain within the 10^{-1}–10^{-2} range, indicating that sufficiently strong media-induced distortions cannot be fully compensated by receiver processing alone. It is important to emphasize that, despite the improvements, the current evaluation still relies on simulations and several idealized assumptions. The channel model assumes known reader sensitivity, flawless writing, a fixed media geometry, and additive Gaussian noise. However, it does not fully account for practical issues such as variations in island size and position caused by fabrication, correlated position jitter, writing errors, track misregistration, reader offset, head skew, sampling timing errors, magnetic property distributions, thermal fluctuations, nonlinear

readback effects, inaccurate channel characterization, and imperfect recording operations. Therefore, the media noise analysis presented in Figure 10 should be viewed as an initial robustness evaluation rather than a complete experimental validation.

Finally, to assess the implementation complexity of the considered receivers, the number of arithmetic operations required to detect one interleaved coded bit was evaluated, as summarized in Table 4. The operation counts include multiplications (Mul.), divisions (Div.), additions (Add.), and subtractions (Sub.) required by the equalizer and detector. The proposed and conventional 1-D DL-PRML receivers have the same arithmetic complexity because they employ the same 11-tap equalizer and 5-tap GPR target. The additional computation introduced by the proposed two-step MMSE method occurs only during coefficient estimation in the design step. It therefore does not increase the per-bit detection complexity during the signal-processing step. Although 0.5Tx oversampling doubles the required processing throughput per bit period, the arithmetic complexity per detected interleaved coded bit remains unchanged. The SOVA detection and LDPC decoding introduce additional latency depending on the traceback depth and number of decoding iterations; however, these components are more common than in 1-D DL-PRML receivers. In contrast, the conventional 2-D DL-PRML receiver requires substantially more arithmetic operations because of its multi-dimensional equalization and detection structure. The proposed receiver provides improved BER performance while retaining the complexity of conventional 1-D DL-PRML processing.

Moreover, to provide a more comprehensive complexity assessment, we also analyze coefficient estimation, processing throughput, memory requirements, and detection latency, as summarized in Table 5; for the 2040-bit sequence with 2× oversampling, the coefficient-estimation sequence contains $K = 4080$ samples. Accumulating the correlation statistics for the 5-tap target and 11-tap equalizer requires an estimated 660,960 multiply-accumulate operations (MACs) per coefficient-estimation run. This estimate excludes the subsequent solution of the 5 × 5 and 11 × 11 systems. The coefficient-estimation cost is incurred offline and is not included in the online operation counts in Table 4.

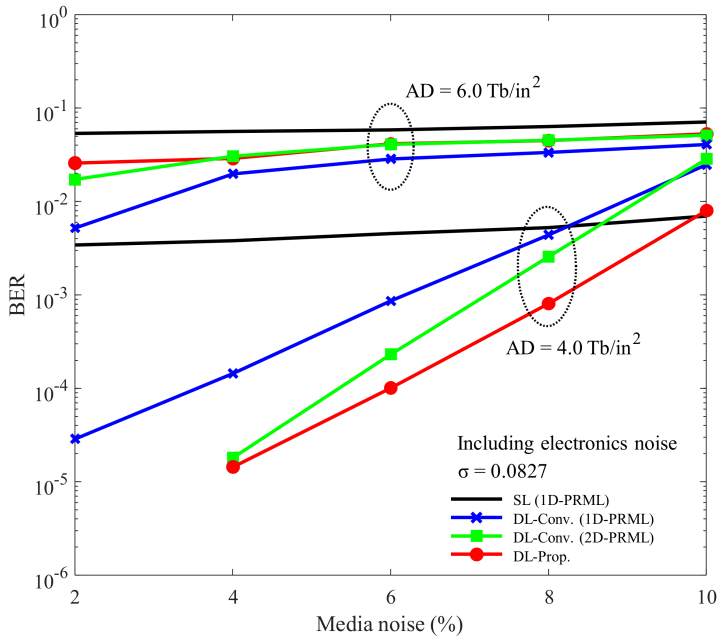


Figure 10. BER performance comparison among the detection techniques considered under different media noise (size- and position-fluctuations) at AD = 4.0 and 6.0 Tbits/in^2 with electronic noise ($\sigma = 0.0827$).

Table 4. Computational complexity of the compared receivers per detected interleaved coded bit.

	Operators	Receivers		
		Conv. 1-D	**Prop. 1-D**	**Conv. 2-D**
Equalizer	Mul./Div.	11	11	21
	Add./Sub.	10	10	21
Detector	Mul./Div.	32	32	2560
	Add./Sub.	64	64	1600
Total	Mul./Div.	43	43	2581
	Add./Sub.	74	74	1621

Table 5. Additional complexity assessment of the proposed 1-D PRML receiver.

Aspects	Assessment
Coefficient estimation	660,960 MACs per run for $K = 4080$; excludes solving the 5×5 and 11×11 systems
Online operations	117 operations per detected interleaved coded bit: 43 Mul./Div. and 74 Add./Sub.
Throughput	Two readback samples per bit period at $0.5T_x$ oversampling
Coefficient storage memory	178 scalar values (712 bytes at 32-bit precision), including correlation matrices, associated vectors, and coefficients; excludes decoder memory
Detection latency	The 5-tap binary target gives 16 trellis states and 32 branches per step; total latency depends on SOVA traceback depth and LDPC decoding iterations

5. Conclusions

This paper presented a co-designed dual-layer bit-patterned magnetic recording (DL-BPMR) framework to improve data-retrieval reliability at areal densities of 2.0–6.0 Tbits/in^2. The proposed approach combines two complementary techniques: controlling head–media spacing (HMS) to strengthen the lower-layer readback signal, and utilizing a combined-processing partial-response maximum-likelihood (PRML) receiver with a two-step minimum mean-square error (MMSE) target and equalizer optimized for staggered dual-layer geometries. The results showed that reducing HMS improved readback separability and balanced the contributions of upper- and lower-layer readback signals, thereby improving signal conditioning for detection. In addition, the proposed receiver consistently achieved lower mean-squared error (MSE) than conventional one-dimensional (1-D) dual-layer processing across the tested signal-to-noise ratio (SNR) range, confirming improved target/equalizer matching under the coupled dual-layer response. In an end-to-end bit-error rate (BER) evaluation, the proposed 1-D DL-BPMR system outperformed the conventional 1-D and two-dimensional dual-layer processing, as well as the 1-D single-layer BPMR baseline, achieving the best performance in the small-HMS regime. Even with media noise factored in, the proposed method still outperformed the others, demonstrating greater robustness under practical recording conditions. Overall, the results confirm that reliable high-density dual-layer retrieval is achievable when the physical readback conditions and receiver design are optimized together.

Author Contributions: Conceptualization, N.R. and C.W.; methodology, N.R. and C.W.; software, N.R. and S.J.G.; validation, C.W., S.J.G. and S.K.; formal analysis, N.R.; investigation, C.W. and S.K.; resources, S.J.G.; data curation, N.R. and S.T.W.; writing—original draft preparation, N.R.; writing—review and editing, N.R., C.W. and S.J.G.; visualization, C.W., S.J.G. and S.K.; supervision, C.W.; project administration, C.W.; funding acquisition, C.W. All authors have read and agreed to the published version of the manuscript.

Funding: The research on "Enhancing Areal Density based on Signal Processing Techniques in Staggered Dual-layer Bit-Patterned Magnetic Recording Systems" (grant number RE-KRIS/FF69/62) by King Mongkut's Institute of Technology Ladkrabang (KMITL) has received funding support from the NSRF.

Institutional Review Board Statement: Not applicable.

Informed Consent Statement: Not applicable.

Data Availability Statement: The original contributions presented in this study are included in the article. Further inquiries can be directed to the corresponding author.

Conflicts of Interest: The authors declare no conflicts of interest.

Appendix A

Here we show step-by-step derivations from the MMSE formulations to the target and equalizer coefficients. The target coefficients are $\mathbf{g}$ (5 taps $\{L_g\}$, monic constraint), and the equalizer coefficients are $\mathbf{f}$ (11 taps $\{L_f\}$).

MMSE-I: We use the raw readback signal to design the target to generate the desired sequence directly, $d_{k'}^{\mathrm{mi}}$.

MMSE-II: We then use the desired sequence, $d_{k''}^{\mathrm{mi}}$, to design the FIR equalizer.

(A) Vector definitions (quantities used in the equations)

(A1) Interleaved input (combined)

Define the interleaved input sequence form from the two-layer coded symbols:

$$a_{2k'}^{mi} = a_{k'}^{up}, a_{2k'+1}^{mi} = a_{k'}^{lw}. \tag{A1}$$

(A2) 5-tap target

$$\mathbf{g} = [g_{-2}\, g_{-1}\, g_0\, g_1\, g_2]^{\mathrm{T}} \in \mathbb{R}^5. \tag{A2}$$

Define the 5-dimensional interleaved column vector of the input sequence for the target:

$$\mathbf{a}_{k''} = \left[a_{k''+2}^{mi}\, a_{k''+1}^{mi}\, a_{k''}^{mi}\, a_{k''-1}^{mi}\, a_{k''-2}^{mi}\right]^{\mathrm{T}} \in \mathbb{R}^5. \tag{A3}$$

Thus, the target (desired/ideal) sequence is

$$d_{k''}^{mi} = \mathbf{g}^{\mathrm{T}}\mathbf{a}_{k''}. \tag{A4}$$

Monic constraint (center main tap):

$$g_0 = 1 \Leftrightarrow \mathbf{I}^{\mathrm{T}}\mathbf{g} = 1, \tag{A5}$$

where

$$\mathbf{I} = [0\,0\,1\,0\,0]^{\mathrm{T}}. \tag{A6}$$

(A3) 11-tap equalizer

With $M = 11$ and $N = 5$,

$$\mathbf{f} = [f_{-5} \ldots f_0 \ldots f_5]^{\mathrm{T}} \in \mathbb{R}^{11} \tag{A7}$$

Define the 11-dimensional column vector of the readback sequence:

$$\mathbf{r}_{k''}^{mi} = \left[r_{k''+5}^{mi} \ \ldots \ r_{k''}^{mi} \ \ldots \ r_{k''-5}^{mi}\right]^{\mathrm{T}} \in \mathbb{R}^{11} \tag{A8}$$

The equalizer output is

$$z_{k''}^{mi} = \mathbf{f}^{\mathrm{T}}\mathbf{r}_{k''}^{mi}. \tag{A9}$$

(B) STEP 1 (MMSE-I): Derive the target g directly from the readback signal

(B1) Define the error and the objective

Since we design the target directly from the raw readback signal, we fit $\mathbf{g}$ so that $d_{k''}^{\mathrm{mi}}$ is close to the readback (with a delay used for alignment). Choose the target delay as the center delay of a 5-tap FIR target:

$$\Delta_t = \frac{L_g - 1}{2} = \frac{5-1}{2} = 2. \tag{A10}$$

Define the MMSE-I error:

$$e_{k''}^{1} = r_{k''-\Delta_t}^{mi} - \mathbf{g}^{\mathrm{T}}\mathbf{a}_{k''} = r_{k''-2}^{mi} - \mathbf{g}^{\mathrm{T}}\mathbf{a}_{k''}. \tag{A11}$$

Formulate MMSE-I:

$$\min_{\mathbf{g}} J_1(\mathbf{g}) = \mathrm{E}\left[\left|e_{k''}^{1}\right|^2\right] \text{ s.t. } \mathbf{I}^{\mathrm{T}}\mathbf{g} = 1. \tag{A12}$$

(B2) Expand $J_1(\mathbf{g})$ into a quadratic form

Start with

$$J_1(\mathbf{g}) = \mathrm{E}\left[\left(r_{k''-2}^{mi} - \mathbf{g}^{\mathrm{T}}\mathbf{a}_{k''}\right)^2\right]. \tag{A13}$$

Expand the square:

$$\left(r - \mathbf{g}^{\mathrm{T}}\mathbf{a}\right)^2 = r^2 - 2r\left(\mathbf{g}^{\mathrm{T}}\mathbf{a}\right) + \left(\mathbf{g}^{\mathrm{T}}\mathbf{a}\right)^2 \tag{A14}$$

Substitute $r = r_{k''-2}^{mi}, \mathbf{a} = \mathbf{a}_{k''}$:

$$J_1(\mathbf{g}) = \mathrm{E}\left[\left(r_{k''-2}^{mi}\right)^2\right] - 2\mathrm{E}\left[r_{k''-2}^{mi}\mathbf{g}^{\mathrm{T}}\mathbf{a}_{k''}\right] + \mathrm{E}\left[\left(\mathbf{g}^{\mathrm{T}}\mathbf{a}_{k''}\right)^2\right]. \tag{A15}$$

Pull $\mathbf{g}$ outside expectations, E (since $\mathbf{g}$ is deterministic during optimization):

$$\mathrm{E}\left[r\mathbf{g}^{\mathrm{T}}\mathbf{a}\right] = \mathbf{g}^{\mathrm{T}}\mathrm{E}[\mathbf{a}r]. \tag{A16}$$

and

$$\left(\mathbf{g}^{\mathrm{T}}\mathbf{a}\right)^2 = \mathbf{g}^{\mathrm{T}}\left(\mathbf{a}\mathbf{a}^{\mathrm{T}}\right)\mathbf{g} \Rightarrow \mathrm{E}\left[\left(\mathbf{g}^{\mathrm{T}}\mathbf{a}\right)^2\right] = \mathbf{g}^{\mathrm{T}}\mathrm{E}\left[\mathbf{a}\mathbf{a}^{\mathrm{T}}\right]\mathbf{g}. \tag{A17}$$

Define the second-order statistics:

$$\mathbf{U} = \mathrm{E}\left[a_{k''}a_{k''}^{\mathrm{T}}\right] \in \mathbb{R}^{5\times5}, \mathbf{p} = \mathrm{E}\left[a_{k''}r_{k''-2}^{mi}\right] \in \mathbb{R}^{5}. \tag{A18}$$

Then

$$J_1(\mathbf{g}) = \underbrace{\mathrm{E}\left[\left(r_{k''-2}^{mi}\right)^2\right]}_{\text{constant}} - 2\mathbf{g}^{\mathrm{T}}\mathbf{p} + \mathbf{g}^{\mathrm{T}}\mathbf{U}\mathbf{g}. \tag{A19}$$

The constant term does not affect the minimizer; hence, the equivalent constrained problem is:

$$\min_{\mathbf{g}} \mathbf{g}^{\mathrm{T}}\mathbf{U}\mathbf{g} - 2\mathbf{g}^{\mathrm{T}}\mathbf{p} \text{ s.t. } \mathbf{I}^{\mathrm{T}}\mathbf{g} = 1. \tag{A20}$$

(B3) Solve with a Lagrangian and obtain the closed-form $\mathbf{g}$

Construct the Lagrangian:

$$\varphi(\mathbf{g}, \lambda) = \mathbf{g}^{\mathrm{T}}\mathbf{U}\mathbf{g} - 2\mathbf{g}^{\mathrm{T}}\mathbf{p} - 2\lambda\left(\mathbf{I}^{\mathrm{T}}\mathbf{g} - 1\right). \tag{A21}$$

Set the gradient with respect to $\mathbf{g}$ to zero.

Differentiate with respect to $\mathbf{g}$ using standard results:

$$\frac{\partial}{\partial \mathbf{g}}\left(\mathbf{g}^{\mathrm{T}}\mathbf{U}\mathbf{g}\right) = 2\mathbf{U}\mathbf{g}(\mathbf{U} \text{ symmetric}), \tag{A22}$$

$$\frac{\partial}{\partial \mathbf{g}}\left(-2\mathbf{g}^{\mathrm{T}}\mathbf{p}\right) = -2\mathbf{p},\ \frac{\partial}{\partial \mathbf{g}}\left(-2\lambda\mathbf{I}^{\mathrm{T}}\mathbf{g}\right) = -2\lambda\mathbf{I}. \tag{A23}$$

Thus,

$$\frac{\partial \varphi}{\partial \mathbf{g}} = 2\mathbf{U}\mathbf{g} - 2\mathbf{p} - 2\lambda\mathbf{I} = 0 \tag{A24}$$

Divide by 2:

$$\mathbf{U}\mathbf{g} = \mathbf{p} + \lambda\mathbf{I}. \tag{A25}$$

Assuming **U** is invertible:

$$\mathbf{g} = \mathbf{U}^{-1}(\mathbf{p} + \lambda\mathbf{I}). \tag{A26}$$

Or:

$$\mathbf{g}^{\mathrm{T}} = (\mathbf{p} + \lambda\mathbf{I})^{\mathrm{T}}\left(\mathbf{U}^{-1}\right)^{\mathrm{T}}. \tag{A27}$$

Determine λ using the monic constraint.
From (A26) apply $\mathbf{I}^{\mathrm{T}}\mathbf{g} = 1$:

$$\mathbf{I}^{\mathrm{T}}\mathbf{U}^{-1}(\mathbf{p} + \lambda\mathbf{I}) = 1, \tag{A28}$$

$$\mathbf{I}^{\mathrm{T}}\mathbf{U}^{-1}\mathbf{p} + \lambda\mathbf{I}^{\mathrm{T}}\mathbf{U}^{-1}\mathbf{I} = 1, \text{and} \tag{A29}$$

$$\lambda = \frac{1 - \mathbf{I}^{\mathrm{T}}\mathbf{U}^{-1}\mathbf{p}}{\mathbf{I}^{\mathrm{T}}\mathbf{U}^{-1}\mathbf{I}}. \tag{A30}$$

Substitute back:

$$\mathbf{g}^{\mathrm{T}} = (\mathbf{p} + \lambda\mathbf{I})^{\mathrm{T}}\left(\mathbf{U}^{-1}\right)^{\mathrm{T}}. \tag{A31}$$

This is the 5-tap target coefficient vector obtained from MMSE-I.

(C) STEP 2 (MMSE-II): Derive the equalizer f (11 taps)

After Step 1, compute the desired sequence:

$$d_{k''}^{mi} = \mathbf{g}^{\mathrm{T}}\mathbf{a}_{k''}. \tag{A32}$$

(C1) Define the error and the objective
Choose the equalizer delay as the center of the 11-tap window:

$$\Delta_e = \frac{L_f - 1}{2} = 5. \tag{A33}$$

Define the MMSE-II error:

$$e_{k''}^2 = d_{k''-\Delta_e}^{mi} - \mathbf{f}^{\mathrm{T}}\mathbf{r}_{k''} = d_{k''-5}^{mi} - \mathbf{f}^{\mathrm{T}}\mathbf{r}_{k''}. \tag{A34}$$

Formulate MMSE-II:

$$\min_{\mathbf{f}} J_2(\mathbf{f}) = \mathrm{E}\left[\left|e_{k''}^2\right|^2\right]. \tag{A35}$$

(C2) Expand
Start with

$$J_2(\mathbf{f}) = \mathrm{E}\left[\left(d_{k''-5}^{mi} - \mathbf{f}^{\mathrm{T}}\mathbf{r}_{k''}\right)^2\right]. \tag{A36}$$

Expand:

$$\left(d - \mathbf{f}^{\mathrm{T}}\mathbf{r}\right)^2 = d^2 - 2d\left(\mathbf{f}^{\mathrm{T}}\mathbf{r}\right) + \left(\mathbf{f}^{\mathrm{T}}\mathbf{r}\right)^2. \tag{A37}$$

Substitute $d = d_{k''-5}^{mi}, \mathbf{r} = \mathbf{r}_{k''}$:

$$J_2(\mathbf{f}) = \mathrm{E}\left[\left(d_{k''-5}^{mi}\right)^2\right] - 2\mathrm{E}\left[\left(d_{k''-5}^{mi}\mathbf{f}^{\mathrm{T}}\mathbf{r}_{k''}\right)\right] + \mathrm{E}\left[\left(\mathbf{f}^{\mathrm{T}}\mathbf{r}_{k''}\right)^2\right]. \tag{A38}$$

Pull $\mathbf{f}$ out:

$$\mathrm{E}\left[d\mathbf{f}^{\mathrm{T}}\mathbf{r}\right] = \mathbf{f}^{\mathrm{T}}\mathrm{E}[\mathbf{r}d] \tag{A39}$$

and

$$\mathrm{E}\left[\left(\mathbf{f}^{\mathrm{T}}\mathbf{r}\right)^2\right] = \mathbf{f}^{\mathrm{T}}\mathrm{E}\left[\mathbf{r}\mathbf{r}^{\mathrm{T}}\right]\mathbf{f}. \tag{A40}$$

Define:

$$\mathbf{R} = \mathrm{E}\left[\mathbf{r}_{k''}\mathbf{r}_{k''}^{\mathrm{T}}\right] \in \mathbb{R}^{11\times 11},\ \mathbf{q} = \mathrm{E}\left[\mathbf{r}_{k''}d_{k''-5}^{mi}\right] \in \mathbb{R}^{11}. \tag{A41}$$

Then:

$$J_2(\mathbf{f}) = \underbrace{\mathrm{E}\left[\left(d_{k''-5}^{mi}\right)^2\right]}_{\text{constant}} - 2\mathbf{f}^{\mathrm{T}}\mathbf{q} + \mathbf{f}^{\mathrm{T}}\mathbf{R}\mathbf{f}. \tag{A42}$$

Drop the constant term:

$$\min_{\mathbf{f}} \mathbf{f}^{\mathrm{T}}\mathbf{R}\mathbf{f} - 2\mathbf{f}^{\mathrm{T}}\mathbf{q}. \tag{A43}$$

(C3) Set the gradient to zero (normal equation)
Compute derivatives:

$$\frac{\partial}{\partial \mathbf{f}}\left(\mathbf{f}^{\mathrm{T}}\mathbf{R}\mathbf{f}\right) = 2\mathbf{R}\mathbf{f},\ \frac{\partial}{\partial \mathbf{f}}\left(-2\mathbf{f}^{\mathrm{T}}\mathbf{q}\right) = -2\mathbf{q}. \tag{A44}$$

Set to zero:

$$2\mathbf{R}\mathbf{f} - 2\mathbf{q} = 0 \Rightarrow \mathbf{R}\mathbf{f} = \mathbf{q}. \tag{A45}$$

Hence:

$$\mathbf{f} = \mathbf{R}^{-1}\mathbf{q}. \tag{A46}$$

Or:

$$\mathbf{f}^{\mathrm{T}} = \mathbf{q}^{\mathrm{T}}\left(\mathbf{R}^{-1}\right)^{\mathrm{T}}. \tag{A47}$$

This is the 11-tap equalizer coefficient vector obtained from MMSE-II.

References

1. Rottmayer, R.; Batra, S.; Buechel, D.; Challener, W.; Hohlfeld, J.; Kubota, Y.; Li, L.; Lu, B.; Mihalcea, C.; Mountfield, K.; et al. Heat-assisted magnetic recording. *IEEE Trans. Magn.* **2006**, *42*, 2417–2421. [CrossRef]
2. Kryder, M.H.; Gage, E.C.; McDaniel, T.W.; Challener, W.A.; Rottmayer, R.E.; Ju, G.; Hsia, Y.-T.; Erden, M.F. Heat assisted magnetic recording. *Proc. IEEE* **2008**, *96*, 1810–1835. [CrossRef]
3. Greaves, S.J.; Suto, H.; Nakamura, Y.; Kanai, Y. Effect of Curie temperature distributions on the user areal density of heat-assisted magnetic recording. *IEEE Trans. Magn.* **2024**, *60*, 3200605. [CrossRef]
4. Zhu, J.-G.; Zhu, X.; Tang, Y. Microwave assisted magnetic recording. *IEEE Trans. Magn.* **2008**, *44*, 125–131. [CrossRef]
5. Chen, W.; Tang, Z.; Kaizu, A.; Kawasaki, S.; Man, K.L.; Mo, C.S.; Roppongi, T.; Dovek, M.M. Spin-torque-oscillator designs in microwave-assisted magnetic recording. In Proceedings of the 2022 IEEE 33rd Magnetic Recording Conference (TMRC), Milpitas, CA, USA, 8–10 August 2022; pp. 1–2. [CrossRef]
6. Takagishi, M. Microwave assisted magnetic recording: Physics and application to hard disk drives. *J. Magn. Magn. Mater.* **2022**, *563*, 169859. [CrossRef]
7. Richter, H.; Dobin, A.; Heinonen, O.; Gao, K.; Veerdonk, R.V.; Lynch, R.; Xue, J.; Weller, D.; Asselin, P.; Erden, M.; et al. Recording on bit-patterned media at densities of 1 Tb/in^2 and beyond. *IEEE Trans. Magn.* **2006**, *42*, 2255–2260. [CrossRef]
8. Nabavi, S.; Kumar, B.V.K.V.; Zhu, J.-G. Modifying Viterbi algorithm to mitigate inter-track interference in bit-patterned media. *IEEE Trans. Magn.* **2007**, *43*, 2274–2276. [CrossRef]
9. Karakulak, S.; Siegel, P.H.; Wolf, J.K.; Bertram, H.N. A new read channel model for patterned media storage. *IEEE Trans. Magn.* **2008**, *44*, 193–197. [CrossRef]
10. Karakulak, S.; Siegel, P.H.; Wolf, J.K. A parametric study of inter-track interference in bit patterned media recording. *IEEE Trans. Magn.* **2010**, *46*, 819–824. [CrossRef]
11. Albrecht, T.R.; Arora, H.; Ayanoor-Vitikkate, V.; Beaujour, J.-M.; Bedau, D.; Berman, D.; Bogdanov, A.L.; Chapuis, Y.-A.; Cushen, J.; Dobisz, E.E.; et al. Bit-patterned magnetic recording: Theory, media fabrication, and recording performance. *IEEE Trans. Magn.* **2015**, *51*, 0800342. [CrossRef]
12. Roddick, E.; Kief, M.; Takeo, A. A new advanced storage research consortium HDD technology roadmap. In Proceedings of the 2022 IEEE 33rd Magnetic Recording Conference (TMRC), Milpitas, CA, USA, 8–10 August 2022; pp. 1–2.

13. Chan, K.S.; Aboutaleb, A.; Sivakumar, K.; Belzer, B.; Wood, R.; Rahardja, S. Data recovery for multi-layer magnetic recording. *IEEE Trans. Magn.* **2019**, *55*, 6701216. [CrossRef]
14. Nakamura, Y.; Nishikawa, M.; Kanai, Y.; Okamoto, Y. A study of three-dimensional equalization for reproducing a double-layer magnetic recording medium. *IEEE Trans. Magn.* **2022**, *58*, 3101804. [CrossRef]
15. Buajong, C.; Warisarn, C. Recording media configurations for double-layered bit-patterned magnetic recording. *AIP Adv.* **2024**, *14*, 015133. [CrossRef]
16. Rueangnetr, N.; Warisarn, C.; Greaves, S.J. Optimization of layer thicknesses for dual-layer bit-patterned media recording (BPMR) systems. *IEEE Trans. Magn.* **2024**, *60*, 3100505. [CrossRef]
17. Nakamura, Y.; Nishikawa, M.; Kanai, Y.; Okamoto, Y. A study of channel time-domain response on equalization for reproducing a double-layer magnetic recording medium. *IEEE Trans. Magn.* **2022**, *58*, 3300105. [CrossRef]
18. Luo, K.; Liao, Y.; Zhang, K.; Jian, Y.; Wang, S.; Chen, J.; Lu, P. On the impact of interlayer misalignment for dual-layer data detection in three dimensional magnetic recording. *J. Magn. Magn. Mater.* **2024**, *610*, 172522. [CrossRef]
19. Nhunork, P.; Warisarn, C.; Tongsomporn, D. An experiment study of head-to-media spacing sensitivity in ultra-high density magnetic recording systems. *Procedia Comput. Sci.* **2016**, *86*, 168–171. [CrossRef]
20. Nguyen, T.A.; Shin, O.-S.; Lee, J. A novel structure and detection for double-layer bit-patterned media recording. *IEEE Access* **2025**, *13*, 182543–182555. [CrossRef]
21. Albuquerque, G.; Hernandez, S.; Kief, M.T.; Mauri, D.; Wang, L. HDD reader technology roadmap to an areal density of 4 Tbpsi and beyond. *IEEE Trans. Magn.* **2022**, *58*, 3100410. [CrossRef]
22. Saito, H. Multidimensional signal processing for high areal density heated-dot magnetic recording. *IEEE Trans. Magn.* **2023**, *59*, 3000810. [CrossRef]
23. Khametong, A.; Warisarn, C. A study of iterative signal processing schemes for double-layered bit-patterned recording. *IEEE Trans. Magn.* **2024**, *60*, 3100305. [CrossRef]
24. Nguyen, T.A.; Lee, J. MAP detection for double-layer bit-patterned media recording. *Appl. Sci.* **2026**, *16*, 155. [CrossRef]
25. Rueangnetr, N.; Koonkarnkhai, S.; Greaves, S.J.; Warisarn, C. Inter-layer interference (ILI) suppression in dual-layer bit-patterned magnetic recording systems. *IEEE Trans. Magn.* 2025, *in press*. [CrossRef]
26. Eleftheriou, E.; Olcer, S. Low-density parity-check codes for digital subscriber lines. In Proceedings of the IEEE International Conference on Communications, New York, NY, USA, 28 April–2 May 2002; Volume 3, pp. 1752–1757.
27. Gallager, R. Low-density parity-check codes. *IEEE Trans. Inf. Theory* **1962**, *8*, 21–28. [CrossRef]
28. Yuan, Z.-M.; Ong, C.L.; Leong, S.H.; Zhou, T.; Liu, B. 3-D sensitivity function of shielded reader by reciprocity principle. *IEEE Trans. Magn.* **2010**, *46*, 1929–1932. [CrossRef]
29. Vucetic, B.; Yuan, J. Trellis-based decoding of linear codes. In *Turbo Codes*; Springer: Boston, MA, USA, 2000; pp. 117–156. [CrossRef]
30. Nabavi, S.; Kumar, B.V.K.V. Two-dimensional generalized partial response equalizer for bit-patterned media. In Proceedings of the 2007 IEEE International Conference on Communications, Glasgow, UK, 24–28 June 2007; pp. 6249–6254. [CrossRef]

Disclaimer/Publisher's Note: The statements, opinions and data contained in all publications are solely those of the individual author(s) and contributor(s) and not of MDPI and/or the editor(s). MDPI and/or the editor(s) disclaim responsibility for any injury to people or property resulting from any ideas, methods, instructions or products referred to in the content.